a comparison of values so obtained with those found by Siegbahn from crystal diffraction, it was possible to calculate the following relation between the relative and absolute units:

$$1 \text{ kX} = 1.00202\text{Å}.$$

This conversion factor was adopted in 1946 by international agreement. Later work improved the accuracy of this factor, and the relation is now believed to be

$$1 \text{ kX} = 1.002056\text{Å}^*. \tag{3-16}$$

Note that this relation is stated in terms of still another unit, the Å* unit, which was introduced because of the still remaining uncertainty in the conversion factor. The difference between Å and Å* is only some five parts per million, and the distinction between the two units is negligible except in work of the very highest accuracy.

The present situation is not entirely clear, but the wavelength tables published by the International Union of Crystallography [Vol. C, G.1], which are reproduced in Appendix 7, are the best available values.

The distinction between kX and Å is unimportant if no more than about three significant figures are involved, because the kX unit is only about 0.2 percent larger than the angstrom. In precise work, on the other hand, units must be correctly stated, and on this point there has been considerable confusion in the past. Some wavelength values published prior to about 1946 are stated to be in angstrom units but are actually in kX units. Some crystallographers have used such a value as the basis for a precise measurement of the lattice parameter of a crystal, and the result has been stated, again incorrectly, in angstrom units. Many published parameters are therefore in error, and it is unfortunately not always easy to determine which ones are and which ones are not. The only safe rule to follow, in stating a precise parameter, is to give the wavelength of the radiation used in its determination. Similarly, any published table of wavelengths can be tested for the correctness of its units by noting the wavelength given for a particular characteristic line, Cu $K\alpha_1$ for example. The wavelength of this line is 1.540562 Å* (1974 value, 1.002056 as conversion factor), 1.54051 Å (1946 value, 1.00202 factor), or 1.53740 kX. See Appendix 7 for the estimated accuracy of the wavelengths listed there.

3-8 DIFFRACTION METHODS

Diffraction can occur whenever Bragg's law, $\lambda = 2d \sin\theta$, is satisfied. This equation puts very stringent conditions on λ and θ for any given crystal. With monochromatic radiation, an arbitrary setting of a single crystal in a beam of x-rays will not in general produce *any* diffracted beams. Some way of satisfying Bragg's law must be devised, and this can be done by continuously varying either λ or θ during the experiment. The ways in which these quantities are varied distinguish three main diffraction methods:

Method	λ	θ
Laue	Variable	Fixed
Rotating-crystal	Fixed	Variable (in part)
Powder	Fixed	Variable

Laue Method

The Laue method was the first diffraction method ever used, and it reproduces von Laue's original experiment. In this method, a beam of white radiation, the continuous spectrum from an x-ray tube, falls on a fixed single crystal. The Bragg angle θ is therefore fixed for every set of planes in the crystal, and each set selects and diffracts that particular wavelength which satisfies Bragg's law for the particular values of d and θ involved. Each diffracted beam thus has a different wavelength.

There are two variations of the Laue method, depending on the relative positions of source, crystal, and film (Fig. 3-9). In each, the film is flat and placed perpendicular to the incident beam. The film in the *transmission Laue method* (the original Laue method) is placed behind the crystal so as to record the beams diffracted in the forward direction. This method is so called because the diffracted beams are partially transmitted through the crystal. In the *back-reflection Laue method* the film is placed between the crystal and the x-ray source, the incident beam passing through a hole in the film, and the beams diffracted in a backward direction are recorded.

In either method, the diffracted beams form an array of spots on the film as shown in Fig. 3-10. This array of spots is commonly called a *pattern*, but the term is not used in any strict sense and does not imply any periodic arrangement of the spots. On the contrary, the spots are seen to lie on certain curves, as shown by the lines drawn on the photographs. These curves are generally ellipses or hyperbolas for transmission patterns [Fig. 3-10(a)] and hyperbolas for back-reflection patterns [Fig. 3-10(b)].

The spots lying on any one curve are reflections from planes belonging to one zone. This is due to the fact that the Laue reflections from planes of a zone all lie

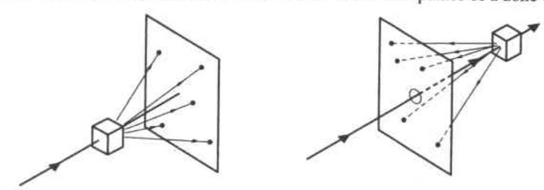

(a) (b)

Figure 3-9 (a) Transmission and (b) back-reflection Laue methods.

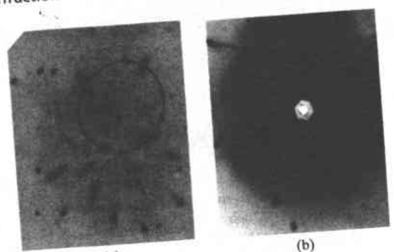

Figure 3-10 (a) Transmission and (b) back-reflection Laue patterns of an aluminum crystal (cubic). Tungsten radiation, 30 kV, 19 mA.

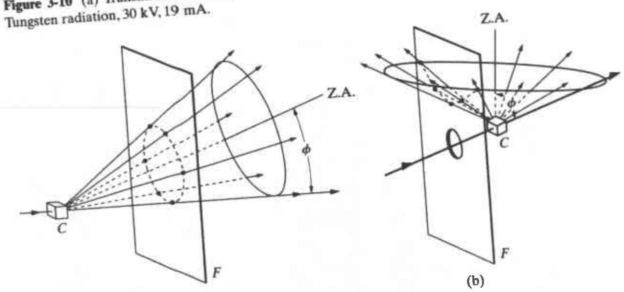

Figure 3-11 Location of Laue spots (a) on ellipses in transmission method and (b) on hyperbolas in back-reflection method. (C = crystal, F = film, Z.A. = zone axis.)

on the surface of an imaginary cone whose axis is the zone axis. As shown in Fig. 3-11(a), one side of the cone is tangent to the transmitted beam, and the angle of inclination ϕ of the zone axis (Z.A.) to the transmitted beam is equal to the semi-apex angle of the cone. A film placed as shown intersects the cone in an imaginary ellipse passing through the center of the film, the diffraction spots from planes of a zone being arranged on this ellipse. When the angle ϕ exceeds 45°, a film placed between the crystal and the x-ray source to record the back-reflection pattern will intersect the cone in a hyperbola, as shown in Fig. 3-11(b).

The fact that the Laue reflections from planes of a zone lie on the surface of a cone can be demonstrated nicely with the stereographic projection. In Fig. 3-12, the crystal is at the center of the reference sphere, the incident beam I enters at the left, and the transmitted beam T leaves at the right. The point representing the zone axis lies on the circumference of the basic circle and the poles of five planes belonging

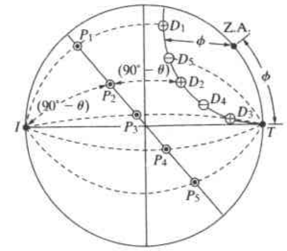

Figure 3-12 Stereographic projection of transmission Laue method.

to this zone, P_1 to P_5, lie on the great circle shown. The direction of the beam diffracted by any one of these planes, for example the plane P_2, can be found as follows. I, P_2, D_2 (the diffraction direction required), and T are all co-planar. Therefore D_2 lies on the great circle through I, P_2, and T. The angle between I and P_2 is $(90° - \theta)$, and D_2 must lie at an equal angular distance on the other side of P_2, as shown. The diffracted beams so found, D_1 to D_5, are seen to lie on a small circle, the intersection with the reference sphere of a cone whose axis is the zone axis.

The positions of the spots on the film, for both the transmission and the back-reflection method, depend on the orientation of the crystal relative to the incident beam, and the spots themselves become distorted and smeared if the crystal has been bent or twisted in any way. These facts account for the two main uses of the Laue methods: the determination of crystal orientation and the assessment of crystal quality.

The Ewald sphere treatment of diffraction of a single wavelength λ from a crystal can be readily extended to the Laue method where multiple λ are incident. The range of wavelengths used is represented by a series of parallel incident beams, each with a different length proportional to $1/\lambda_i$. Note that each of these vectors terminates at the origin of the reciprocal lattice, and each has a different origin (Fig. 3-13). Thus, each incident beam $\mathbf{S}_o/\lambda_i$ has a corresponding Ewald sphere touching the origin of the reciprocal lattice and having radius $1/\lambda_i$. All of the different $\mathbf{S}_o/\lambda_i$ pass through the origin of the reciprocal lattice, and the corresponding Ewald spheres have centers lying on the line **OACDB** of Fig. 3-13, i.e., the incident beam direction. The range of wavelengths present in the incident beam is of course not infinite. It has a sharp lower limit at λ_{SWL}, the short-wavelength limit of the continuous spectrum; the upper limit is less definite and depends on experimental factors such as whether the transmission or back-reflection geometry is being used. In the example of the Ewald sphere construction shown in Fig. 3-13, the upper wavelength limit is taken as the wavelength of the K absorption edge of the silver in the emulsion (0.48 Å), because the effective photographic intensity of the continuous spectrum drops abruptly at that wavelength [see Fig. 7-5]. This choice is most appropriate for transmission Laue patterns of crystals which are quite absorbing since the

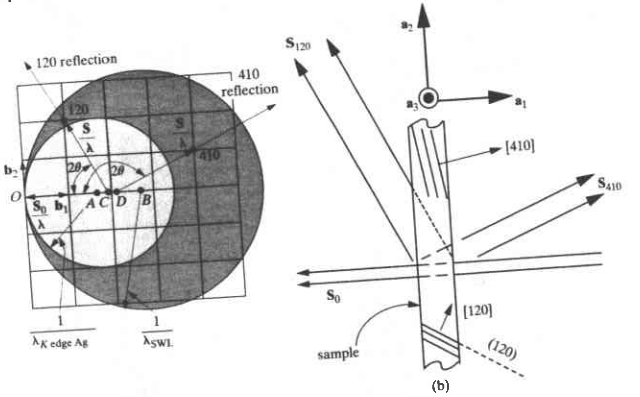

Figure 3-13 Reciprocal lattice (a) and corresponding schematic of the crystal in direct space (b) for the Laue method. $(\mathbf{S}-\mathbf{S}_0)/\lambda = \mathbf{H}$.

value of the linear attenuation coefficient (of an element in a sample) rises rapidly with increasing wavelength. For back-reflection Laue patterns considerable darkening of the film wll occur for wavelengths above the silver edge and below the bromine K-edge as well as for somewhat longer wavelengths.

To these two extreme wavelengths correspond two extreme Ewald spheres, as shown in Fig. 3-13, which is a section through these spheres and the $l = 0$ layer of the reciprocal lattice. The incident beam is along the $\mathbf{b}_1$ vector, i.e., perpendicular to the ($h00$) planes of the crystal. The larger sphere shown is centered at B and has a radius equal to the reciprocal of λ_{SWL}, while the smaller sphere is centered at A and has a radius equal to the reciprocal of the wavelength of the silver K absorption edge. A whole series of spheres lie between these two, and any reciprocal-lattice point lying in the shaded region of the diagram is on the surface of one of these spheres and corresponds to a set of crystal planes oriented to diffract one of the incident wavelengths. In the forward direction, for example, a 120 reflection will be produced. To find its direction, locate a point C on AB which is equidistant from the origin O and the reciprocal-lattice point 120; C is therefore the center of the Ewald sphere passing through the point 120. Joining C to 120 gives the diffracted-beam vector $\mathbf{S}/\lambda$ for this reflection. The direction of the 410 reflection, one of the many backward-diffracted beams, is found in similar fashion; here the reciprocal-lattice point in question is situated on a Ewald sphere centered at D.

Rotating-Crystal Method

In the rotating-crystal method a single crystal is mounted with one of its axes, or some important crystallographic direction, normal to a monochromatic x-ray beam. A cylindrical film is placed around it and the crystal is rotated about the chosen direction, the axis of the film coinciding with the axis of rotation of the crystal (Fig. 3-14). As the crystal rotates, a particular set of lattice planes will, for an instant, make the correct Bragg angle for diffraction of the monochromatic incident beam, and at that instant a diffracted beam will be formed. The diffracted beams are again located on imaginary cones but now the cone axes coincide with the rotation axis. The result is that the spots on the film, when the film is laid flat, lie on imaginary horizontal "layer" lines, as shown in Fig. 3-15. Since the crystal is rotated about only one axis, the Bragg angle does not take on all possible values between 0° and 90° for every set of planes. Not every set, therefore, is able to produce a diffracted beam; sets perpendicular or almost perpendicular to the rotation axis are examples.

The Ewald sphere construction for monochromatic radiation can be used to illustrate why beams diffracted from a single crystal rotated about one of its axes lie on the surface of cones coaxial with the rotation axis. This interpretation of the patterns of diffraction spots was emphasized by Bernal [3.10]. Suppose a simple cubic crystal is rotated about the axis [001]. This is equivalent to rotation of the reciprocal lattice about the $\mathbf{b}_3$ axis. Figure 3-16 shows a portion of the reciprocal lattice oriented in this manner, together with the adjacent Ewald sphere.

All crystal planes having indices ($hk1$) are represented by points lying on a plane (called the "$l = 1$ layer") in the reciprocal lattice, normal to $\mathbf{b}_3$. When the reciprocal lattice rotates, this plane cuts the Ewald sphere in the small circle shown, and any points on the $l = 1$ layer which touch the sphere surface must touch it on this circle. Therefore all diffracted-beam vectors $\mathbf{S}/\lambda$ must end on this circle, which is equiva-

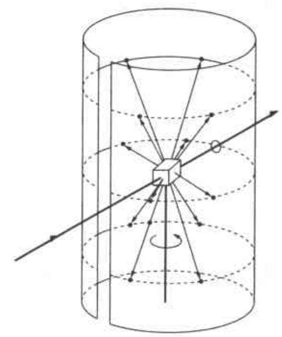

Figure 3-14 Rotating-crystal method.

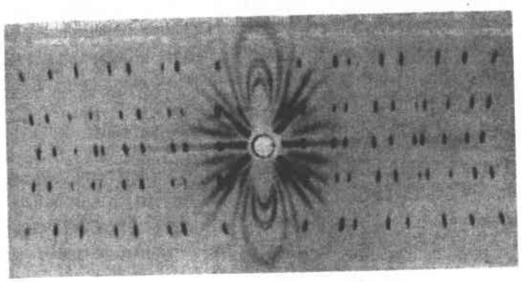

Figure 3-15 Rotating-crystal pattern of a quartz crystal (hexagonal) rotated about its c axis. Filtered copper radiation. (The streaks are due to the white radiation not removed by the filter.) (Courtesy of B. E. Warren.)

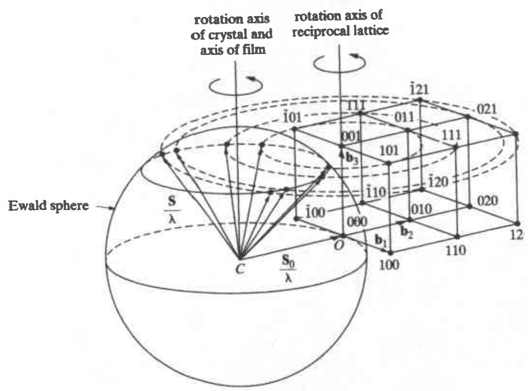

Figure 3-16 Reciprocal-lattice treatment of rotating-crystal method.

lent to saying that the diffracted beams must lie on the surface of a cone. In this particular case, all the *hk*1 points shown intersect the surface of the sphere sometime during their rotation about the $\mathbf{b}_3$ axis, producing the diffracted beams shown in

Fig. 3-16. In addition many *hk0* and *hk*1 reflections would be produced, but these have been omitted from the drawing for the sake of clarity.

The chief use of the rotating-crystal method and its variations were in the determination of unknown crystal structures, but the complete determination of complex crystal structures is a subject beyond the scope of this book and outside the province of the average materials scientist/engineer who uses x-ray diffraction as a laboratory tool. Analyzing patterns consisting of layer lines of diffraction spots remains important however, for polymers and is covered in Chap. 18.

Powder Method

In the powder method, the crystal to be examined is reduced to a very fine powder or already is in the form of loose or consolidated microscopic grains. The sample in a suitable holder is placed in a beam of monochromatic x-rays. Each particle of the powder is a tiny crystal, or assemblage of smaller crystals, oriented at random with respect to the incident beam. Just by chance, some of the crystals will be correctly oriented so that their (100) planes, for example, can diffract the incident beam. Other crystals will be correctly oriented for 110 reflections, and so on. The result is that every set of lattice planes will be capable of diffraction. The mass of powder is equivalent, in fact, to a single crystal rotated, not about one axis, but about all possible axes.

Consider one particular *hkl* reflection, and remember that $\mathbf{S}$, $\mathbf{S}_0$ and $\mathbf{N}_{hkl}$, the normal to the diffraction planes (*hkl*), must be coplanar. One or more little crystals will, by chance, be so oriented that their (*hkl*) planes make the correct Bragg angle for diffraction; Fig. 3-17(a) shows one plane in this set and the diffracted beam formed. If this plane is now rotated about the incident beam in such a way that θ is kept constant, then the diffracted beam will travel over the surface of a cone as shown in Fig. 3-17 (b), the axis of the cone coinciding with the transmitted beam. Equivalently, one can imagine rotating N_{hkl} about $\mathbf{S}_0$ while keeping the angle between them equal to $90° - \theta$ degrees.

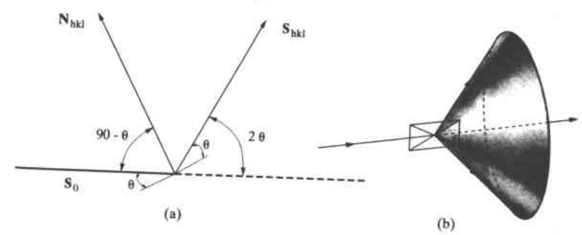

Figure 3-17 Formation of a diffracted cone of radiation in the powder method.

This rotation does not actually occur, but the presence of a large number of crystal particles having all possible orientations is equivalent to this rotation, since among these particles there will be a certain fraction whose (hkl) planes make the correct Bragg angle with the incident beam and which at the same time lie in all possible rotational positions about the axis of the incident beam. The hkl reflection from a stationary mass of powder thus has the form of a conical sheet of diffracted radiation, and a separate cone is formed for each set of differently spaced lattice planes.

Figure 3-18 shows three such cones and also illustrates a common powder-diffraction method. In this, the Hull/Debye–Scherrer method [3.11, 3.12], a narrow strip of film is curved into a short cylinder with the specimen placed on its axis and the incident beam directed at right angles to this axis.[8] The cones of diffracted radiation intersect the cylindrical strip of film in lines, and when the strip is unrolled and laid flat, the resulting pattern appears as in Fig. 3-18(b). Actual patterns, produced by various metal powders, are shown in Fig. 3-19. Each diffraction line is made up of a large number of small spots, each from a separate crystal particle, the spots lying so close together that they appear as a continuous line. The lines are generally curved, unless they occur exactly at $2\theta = 90°$ when they will be straight. From the measured position of a given diffraction line on the film, θ can be determined, and from θ, knowing λ, the spacing d of the diffracting lattice planes which produced the line.

Conversely, if the shape and size of the unit cell of the crystal are known, the position of all possible diffraction lines on the film can be predicted. The line of lowest 2θ value is produced by diffraction from planes of the greatest spacing. In the cubic system, for example, d is a maximum when $(h^2 + k^2 + l^2)$ is a minimum, and the minimum value of this term is l, corresponding to (hkl) equal to (100). The 100 reflection is accordingly the one of lowest 2θ value. The next possible reflection will have indices hkl corresponding to the next higher value of $(h^2 + k^2 + l^2)$, namely 2, in which case (hkl) equals (110), and so on.

The reciprocal lattice of a randomly oriented powder sample consists of a series of reciprocal lattice (rel) shells centered on the origin of the reciprocal lattice. Remembering that all orientations are equally likely for a random powder sample, constructing the reciprocal lattice representing the powder is straight-forward: first draw the reciprocal lattice for a single grain and second rotate the reciprocal lattice points through all possible orientations. Each reciprocal lattice point hkl for the crystal becomes, therefore, a sphere of radius $1/d_{hkl}$, centered on the reciprocal lattice origin (Fig. 3-20a). For an incident beam $\mathbf{S}_0$ and Bragg angles θ_{hkl}, a number of $\mathbf{S}_{hkl}$ simultaneously satisfy Bragg's law. The loci of $\mathbf{S}_{hkl}$ are determined by the intersection of the rel shells and the Ewald sphere and consist of a series of cones cen-

[8] Most authors term this technique the Debye–Scherrer method, but it seems reasonable to acknowledge the independent and more-or-less simultaneous development in the US and Germany during the First World War.

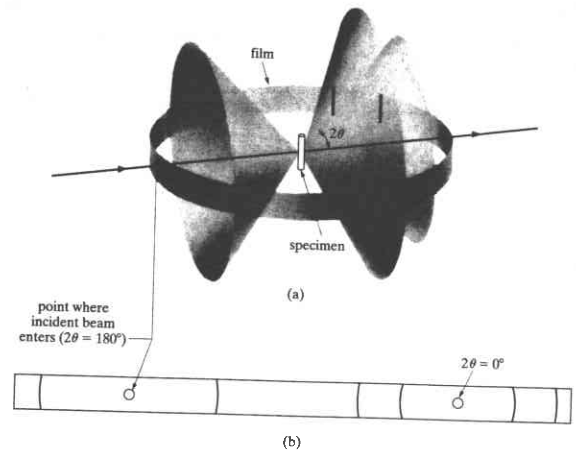

Figure 3-18 Hull/Debye–Scherrer powder method: (a) relation of film to specimen and incident beam; (b) appearance of film when laid flat.

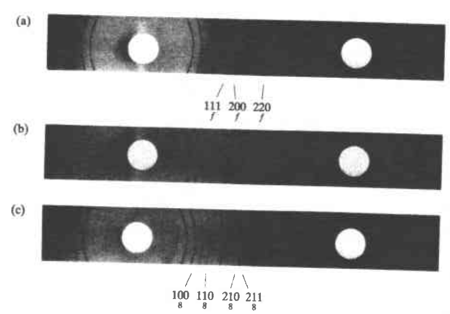

Figure 3-19 Hull/Debye–Scherrer powder patterns of copper (FCC), tungsten (BCC), and zinc (HCP). Filtered copper radiation, camera diameter = 5.73 cm.

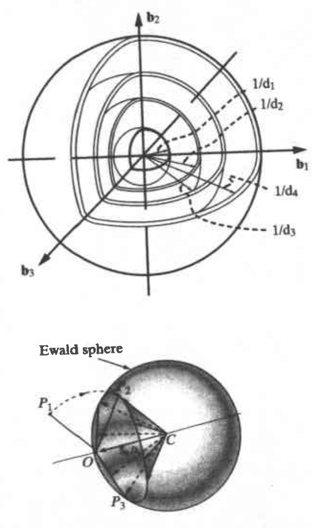

(a)

(b)

Figure 3-20 (a) Reciprocal lattice shells with radii $1/d_1$, $1/d_2$, $1/d_3$ and $1/d_4$, and (b) diffraction cones from the intersection of a reciprocal lattice shell and the Ewald sphere. When P_1 is rotated about the reciprocal lattice origin, it intersects the Ewald sphere at P_2, P_3 and other points of a circle.

tered on $\mathbf{S}_0$ (diffraction in the forward direction) or on $-\mathbf{S}_0$ (diffraction in back-reflection). The formation of one such cone is illustrated in Fig. 3-20b, but for clarity the Ewald sphere is pictured and the reciprocal lattice shells are omitted. Instead, reciprocal lattice point P on one shell is rotated through all possible orientations. The resulting intersection of the shell and the Ewald sphere is a circle, and the locus of $\mathbf{S}_{hkl}$ is a cone.

The x-ray spectrometer can be used as a tool in diffraction analysis. This instrument is known as a *diffractometer* when it is used with x-rays of *known* wave-length to determine the *unknown* spacing of crystal planes [3.13], and as a spectrometer in the reverse case, when crystal planes of known spacing are used to determine unknown wavelengths. The diffractometer is always used with monochromatic radiation and measurements may be made on either single crystals or polycrystal line

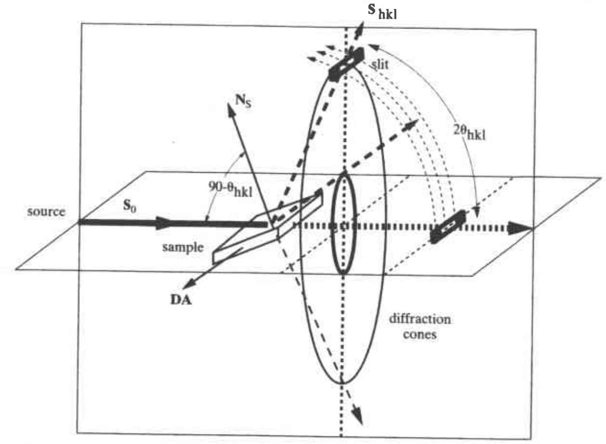

Figure 3-21 Illustration of the role of the slit on the detector in measuring diffraction peaks in powder diffractometry. Two diffraction cones are shown, $\mathbf{N}_S$ is the normal to the sample, **DA** is the diffractometer rotation axis; and $\mathbf{S}_0$, $\mathbf{N}_S$ and the portions of $\mathbf{S}_1$ and $\mathbf{S}_2$ (portions of the cones intersecting the slit) are coplanar.

specimens (early developments are outline in [G.17 and G.18]), the detector intercepts and measures only a short arc of any one cone of diffracted rays (Fig. 3-21). Note that the diffractometer's receiving slit is essential to the observation of diffraction peaks of randomly-oriented, fine-grained powders. The diffraction cones are always present; in fact, cones for all possible *hkl* are present simultaneously. The receiving slit is necessary to eliminate all diffracted radiation except that passing through this very narrow angular window.

Different powder diffraction techniques sample different portions of reciprocal space, and a complete understanding of diffraction phenomena from a reciprocal space perspective requires rigorous definition of the reciprocal space sampling region for each technique. Developing such an understanding is beyond the scope of this book, and the reader is referred to more comprehensive treatments of reciprocal space [3.5].

The Hull/Debye–Scherrer and other camera methods and the diffractometer are very widely used. Powder diffraction is, of course, the only method that can be employed when a single-crystal specimen is not available, and this is the case more often than not in materials work. The method is especially suited for determining lattice parameters with high precision and for the identification of phases, whether they occur alone or in mixtures such as polyphase alloys, corrosion products, refractories, and rocks. These and other uses of the powder diffraction will be fully described in later chapters.

3-9 EXPERIMENTAL VISUALIZATION OF THE RECIPROCAL LATTICE

The preceding section discussed how the rotating crystal method allowed imaging of the distribution of reciprocal lattice points in space. Transmission electron microscopy (TEM) also images the reciprocal lattice directly: planes through the reciprocal lattice can be seen in certain TEM operating modes. In TEM there are a series of three or more lenses following the sample and providing the high magnifications which make the TEM so useful for materials characterization. The wave-like properties of electrons allow them to diffract from crystalline samples. Typically in TEM, electrons are accelerated to 100 keV or higher and have wavelengths of 0.037 Å or lower. This acceleration allows the electrons to be transmitted through samples whose thicknesses are on the order of 1000 Å. Because electrons carry a charge, magnetic lenses are effective at focusing electrons (unlike the case of x-rays where lenses can deflect the photons only a minescule fraction of a degree.) It is important to note that most materials' TEM imaging of materials relies on diffracted electrons to provide image contrast.

The very small wavelength of the electrons means that the radius of the corresponding Ewald sphere is very large compared to the spacing between reciprocal lattice points or compared to the Ewald sphere diameter for x-rays. For 0.037 Å radiation, the Ewald sphere radius is 25 $Å^{-1}$ compared to ~1 $Å^{-1}$ for x-rays and to ~0.5 $Å^{-1}$ for the reciprocal lattice spacing. This means that the curvature of the Ewald sphere is gradual compared to the reciprocal lattice spacings, and that, in the vicinity of the origin of the reciprocal lattice, the Ewald sphere is essentially a plane cutting through the reciprocal lattice (Fig. 3-22). As will be seen in Ch. 4, the sample's thinness produces reciprocal lattice points which are elongated along the thin axis of the sample, i.e., rel rods or reciprocal lattice rods, and the rods intersect the Ewald sphere over quite a large range of 1/d. This section of the reciprocal lattice

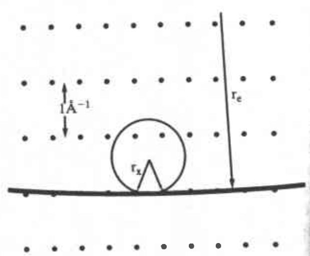

Figure 3-22 Reciprocal lattice of the orthorhombic crystal shown in Fig. 3-6 with the Ewald spheres and radii r_x for Cu *Kα* x-rays and r_e for 100 keV electrons.

imaged by the TEM is termed a diffraction pattern and is normally identified by the direction of incidence of the electrons, i.e., by the normal to the reciprocal lattice plane.

The TEM ray diagram pictured in Fig. 3-23 shows how an image of the sample or an image of the sample's diffraction pattern is obtained. The incident electrons are indicated by the arrows at the top of the figure, and one diffracted beam **G** and the transmitted beam **O** originating from each of three points (A, B and C) in the sample illustrate the electron-sample interactions of interest here. The diffracted and transmitted beams pass through the objective lens whose optic axis is **BB**´. Parallel rays are brought to a focus in the diffraction plane, and rays diverging from a point are recombined in the image plane. In other words, the three rays **G** from A, B and C are combined at G in the diffraction plane, and the rays **G** and **O** from A recombine at A´ in the image plane. If the other lenses of the TEM are focussed on the diffraction plane, the essentially planar section of the reciprocal lattice is imaged. If focussing is on the image plane, an image of the sample results. In other words, parallel directions are mapped onto a single point in the diffraction plane in just as all (*hkl*) in direct space were mapped onto point *hkl* in reciprocal space (Sec. 2-4).

Figure 3-24 shows a diffraction pattern recorded from a grain of NiAl with the electron beam parallel to [100]. The four-fold symmetry expected along <100> in the CsCl structure is clearly seen. Multiple orders of each diffraction vector are seen simultaneously, an apparent contradiction of Bragg's law: for a single wavelength Bragg's law predicts that first and second order diffraction (*hkl* and *2h 2k 2l*) occur at angles θ_{hkl} and θ_{2h2k2l} given, for cubic axial systems, by

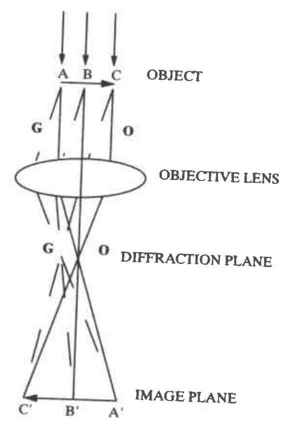

Figure 3-23 TEM ray diagram showing the diffraction plane and image plane.

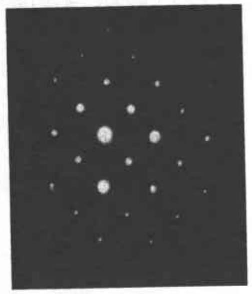

Figure 3-24 001 diffraction pattern from a grain of NiAl. The indices for each diffraction spot are given in Fig. 20-6.

$$\sqrt{2}\sin\theta_{hkl} = \sin\theta_{2h2k2l}.$$

The question is how first and second order diffraction can occur simultaneously for the same angle of incidence of $\mathbf{S}_0$ if small rotations from the Bragg angle destroy constructive interference. Stated in other terms, the derivation of Bragg's law implicitly assumed that the diffraction peaks are delta functions, i.e., that the crystal has an infinitely narrow range of reflection.

The resolution to this apparent contradiction lies in the fact that *Bragg's law describes diffraction incompletely*. As will be seen in Chap. 5, very small crystal or grain dimensions have very wide diffraction ranges as a direct consequence of their small size. In other words, significant diffracted intensity occurs at angles off the exact Bragg condition, but development of an understanding of the factors governing diffracted intensity must precede discussion of how far a crystal must rotate before diffracted intensity drops to zero.

3-10 DIFFRACTION UNDER NONIDEAL CONDITIONS

In Sec 3-9, the discussion of diffraction patterns illustrated one consequence of deviation for "ideality". Before going any further, it is important to consider other aspects of the derivation of Bragg's law given in Sec. 3-2 in order to understand precisely under what conditions it is strictly valid. In the derivation certain ideal conditions were assumed, namely a perfect crystal and an incident beam composed of perfectly parallel and strictly monochromatic radiation. These conditions never actually exist. For example, the incident x-ray beam in most powder diffractometers is divergent and the characteristic lines from x-ray tubes have finite spectral widths. Also implicit is that once x-ray photons are diffracted they will not be re-directed; this assumption, the basis of kinematical diffraction theory, holds except for diffraction from thick, highly perfect crystals.

Imperfections in the crystal(s) making up a sample can broaden the diffraction peaks. Only the infinite crystal is really perfect and small size alone, of an otherwise

perfect crystal, can be considered a crystal imperfection, and can lead to peak broadening. The presence of large numbers of dislocations (i.e., strain) in the grains of a sample can produce significant peak broadening. The inference of sample strain or crystallite size from peak widths (or shapes) is an important part of diffraction analysis of materials, and these topics are developed in Chap. 5 and applied to materials analysis in Chap. 14.

PROBLEMS

3-1 A transmission Laue pattern is made of a cubic crystal having a lattice parameter of 4.00 Å. The x-ray beam is horizontal. The $[0\bar{1}0]$ axis of the crystal points along the beam towards the x-ray tube, the $[\bar{1}00]$ axis points vertically upward, and the [001] axis is horizontal and parallel to the photographic film. The film is 5.00 cm from the crystal.

a) What is the wavelength of the radiation diffracted from the $(3\bar{1}0)$ planes?

b) Where will the $3\bar{1}0$ reflection strike the film?

***3-2** A transmission Laue pattern is made of a cubic crystal in the orientation of Prob. 3-1. By means of a stereographic projection similar to Fig. 3-12, show that the beams diffracted by the planes $(\bar{2}\bar{1}0)$, $(\bar{2}\bar{1}3)$, and (211), all of which belong to the zone $[\bar{1}20]$, lie on the surface of a cone whose axis is the zone axis. What is the angle ϕ between the zone axis and the transmitted beam?

3-3 Determine, and list in order of increasing angle, the values of 2θ and (hkl) for the first three lines (those of lowest 2θ values) on the powder patterns of substances with the following structures, the incident radiation being Cu $K\alpha$:

a) simple cubic ($a = 3.00$ Å),

b) simple tetragonal ($a = 2.00$ Å, $c = 3.00$ Å),

c) simple tetragonal ($a = 3.00$ Å, $c = 2.00$ Å),

d) simple rhombohedral ($a = 3.00$ Å, $\alpha = 80°$).

3-4 Plot the reciprocal lattice for a polycrystalline sample of a material with a simple tetragonal structure and lattice parameters $a = 4.0$ Å and $c = 5.0$ Å. (Use a two-dimensional section through the three-dimensional space).

3-5 Sketch the Ewald sphere construction for 200 diffraction with Mo $K\alpha$ radiation and a polycrystalline specimen of a simple cubic substance with $a = 3.30$ Å. Graphically determine the angular rotation required to orient the sample for 300 diffraction if a $\theta - 2\theta$ diffractometer is being used.

3-6 Diffractometers typically can scan up to, but not beyond, 165° 2θ. For the sample in Problem 3-4, what are the indices (i.e., hkl) of the highest angle reflection if (a) Ag $K\alpha$ radiation is used, (b) Cu $K\alpha$ radiation is used and c) Cr $K\alpha$ radiation is used?